Quantifying Wind Turbine Blade Surface Roughness using Sandpaper Grit Sizes: An Initial Exploration

Ivan Nikolov and Claus Madsen
Department of Architecture, Design and Media Technology, Aalborg University, Rendsburggade 14, Aalborg, Denmark

Keywords: 3D Reconstruction, Surface Inspection, Sandpaper Roughness, Classification, Random Forests, Geometrical Properties.

Abstract: Surface inspection of wind turbine blades is a necessary step, to ensure longevity and sustained high energy output. The detection of accumulation of damages and increased surface roughness of in-use blades, is one of the main objectives of inspections in the wind energy industry. Creating 3D scans of the leading edges of blade surfaces has been more and more used for capturing the roughness profile of blades. An important part in analysing these surface 3D scans is the standardization of the captured data across different blade surfaces, types and sizes. In this paper we propose an initial exploration of using sandpaper grit sizes to provide this standardization. Sandpaper has been widely used for approximating different levels of blade surface roughness and its standardized nature can be used to easily describe and compare blade surfaces. We reconstruct a number of different sandpaper grit sizes - from coarser P40 to a finer P180. We extract a number of 3D surface features from them and use them to train a random forest classification method. This method is then used to segment the surfaces of wind turbine blades in areas of different surface roughness. We test our proposed solution on a variety of blade surfaces - from smooth to course and damaged and show that it manages to classify them depending on their roughness.

1 INTRODUCTION

Surface inspection is a required part of ensuring the proper working condition of machinery and infrastructure in industries like agriculture (El-Mesery et al., 2019), manufacturing (Dastoorian et al., 2018) and energy production (Zhang et al., 2017b) among other. The wind energy production industry is particularly susceptible to the effects of infrastructure damages and degradation. For achieving maximum wind turbine performance, blades need to be inspected regularly and potential damages caused by weather erosion and imperfections in the manufacturing process (Martin et al., 2018), (Du et al., 2020), need to be detected as soon as possible. It has been shown that the presence of even small surface roughness deviations and damages can cause 2% and 5% loss in energy production (Langel et al., 2015), with numbers as high as 25% for larger damages and surface imperfections (Schramm et al., 2017).

Wind turbine blade inspection is normally focused on the leading edge of the blades, as it is shown that damages there affect performance the most (Bak et al., 2016). Inspection can be done manually by experts on site or in a laboratory setting through contact measurements and microscopy analysis (Chen, 2018) or by using machine vision methods (Shihavuddin et al., 2019). This normally requires capturing images of the surface, which are used for detecting potential damages and imperfection (Shihavuddin et al., 2019), (Moreno et al., 2018), (Al-Kaff et al., 2017). These algorithms require a lot of image data of both clean and damaged surfaces of wind turbine blades, which is not easily accessible. These systems also cannot normally quantify the micro surface roughness of the blade, as they lack depth information. This depth information can be captured by reconstructing the 3D surface, using techniques like Structure from Motion (Zhang et al., 2020), (Nielsen et al., 2020).

To quantify this information and be able to compare it between blade surfaces, a standardized model of measurement of surface roughness is required. Profile roughness metrics part of the ISO 4287 (ISO4287, 1997) standard are used for estimation of the details of line scans of surfaces. These profile metrics can be extended to a 3D area, by using the ISO 25178 (ISO25178, 2012) standard. For 3D, a plane is fitted to the surface patches and the metrics are cal-

Nikolov, I. and Madsen, C.
Quantifying Wind Turbine Blade Surface Roughness using Sandpaper Grit Sizes: An Initial Exploration.
DOI: 10.5220/0010283908010808
In *Proceedings of the 16th International Joint Conference on Computer Vision, Imaging and Computer Graphics Theory and Applications (VISIGRAPP 2021) - Volume 5: VISAPP*, pages 801-808
ISBN: 978-989-758-488-6

culated from their values. In this paper we explore extending these metrics representations, by classifying the surface based on sandpaper roughness that best describes it. Sandpapers with different grit sizes have been widely used in the literature for modeling wind turbine blade roughness in wind tunnels (Marzuki et al., 2018), (Genc et al., 2019). It has been shown that surfaces with attached sandpaper patches exhibit the same behaviour as damaged ones. By classifying wind turbine blades, into different sandpaper roughness profiles, their degradation can be more easily communicated and compared between blades. In addition, sandpaper surface grits are standardized (ISO6344, 1998) and easily accessible, making reproduction of results easy and straightforward. Finally, 3D data of sandpaper surfaces can be much more easily obtained, than real wind turbine blade surface data with different levels of surface damages.

2 STATE OF THE ART

Wind turbine blade analysis can be used to calculate the predicted energy production (Han et al., 2018) and the utilization coefficients of turbines (Wang and Zhang, 2017). It can be also used for introducing a more granular control on the flow control and aerodynamic properties of blades (Langel et al., 2017).

Capturing of 3D data from the surface of wind turbine blades is a widely researched topic. Two main approaches to capturing 3D can be seen in the state of the art - for on-site inspections (Xu et al., 2019), when the wind turbine has been just stopped and offline laboratory inspections, where decommissioned blades are normally inspected (Chen, 2018). The first type of inspection is performed on a more regular basis and aims to keep the blades in as close as possible optimal conditions, while the second type is focus on understanding why and how a blade failed or it was decided that the damages are too severe. For on-site inspections cameras and 3D sensors like LiDARs and stereo cameras are mounted on unmanned aerial vehicles (Zhang et al., 2017a), (Peng and Liu, 2018). These aim to produce less high detailed reconstructions, which could under optimal capturing conditions capture enough information to give an estimate of the current condition of the blades. Laboratory inspections normally use more detailed surface analysis technique, employing electronic microscopes or surface probes (Chan et al., 2019), (Amenabar et al., 2011). These methods can capture very high resolution sub-millimeter accuracy reconstructions of the blade surfaces.

In this paper we try to classify wind turbine blade surfaces using sandpapers with different grit sizes. As sandpapers have known surface properties, we can then infer the same information about the blade surfaces. In addition, sandpaper data is widely used for simulating how different surface roughness affects the aerodynamic characteristics of wind turbine blades and their energy production potential. We base our research on traditional supervised learning methods, using hand crafted features like the ones presented in the work of (Weinmann et al., 2015), (Hackel et al., 2016), (Dittrich et al., 2017), for use on large scale LiDAR point cloud segmentation, focusing on extracting geometrical features, which describe the underlying surface in a robust way. Our proposed solution uses 3D sandpaper data to train a Random Forest classifier, which is later used to segment wind turbine blade surfaces into ares best described by the different sandpaper grit sizes This information can be later used to model test setups or to better evaluate how the roughness would affect the blade, based on sandpaper wind tunnel tests. We show that the proposed approach gives promising results.

3 METHODOLOGY

3.1 SfM Overview

As both the sandpaper patches and the testing wind turbine data are captured using Structure from Motion (SfM), we will first give an overview of the method, for easier reproducibility. SfM is a part of the multi-view stereo algorithms, that uses only 2D image data from different positions and view directions to reconstruct the full 3D surface of an object (Ozyesil et al., 2017). A number of images with a certain overlap are used as input to the algorithm. Features are extracted from each image and matched between images. This can be done using algorithms like SIFT (Lowe, 2004) or ORB (Rublee et al., 2011). These matched features, together with information about the intrinsic parameters of the camera used to take the images, are used to iteratively triangulate the camera positions and create a sparse point cloud of the scanned object. The sparse point cloud is then refined using bundle adjustment (Triggs et al., 1999) and a dense point cloud is created from the 3D sparse points and camera positions.

3.2 Sandpaper 3D Reconstruction

A number of sandpaper grit sizes are chosen for developing the training examples and given in Table 1, to-

Table 1: Sandpaper grit size and the nominal average particle diameter in *mm* (FEPA, 1955).

Grit size	Nom. av. diam. (*mm*)
P40	0.425
P60	0.269
P80	0.201
P100	0.162
P120	0.125
P180	0.082

gether with their average particle size. This standard is proposed by (FEPA, 1955) and widely used. The "P" notation of the grit sizes is inversely related to the coarseness of the sandpaper material and represents the size of the particles, embedded in the material. These grit sizes are chosen, because they are widely used for blade roughness approximation (Genc et al., 2019) and the nominal average diameter of their grit structure is representative of blade roughness values, at which energy production loss starts to be observed (Bak et al., 2016). To more closely mimic how roughness on a wind turbine blade edge would behave, the sandpaper patches are mounted on blade replicas made from styrofoam. The replicas are modeled after the NACA 633418 blade and can be seen in Figure 1(a).

For 3D reconstructing the blade replicas a Canon 5Ds camera is used. As proposed by (Nikolov and Madsen, 2016), a semi-circular pattern with a 1.5m radius is used and 18 images are taken in three different heights of the leading edge with the sandpaper attached. The thus created 54 images are then used as an input to Metashape (Agisoft, 2010), a commercial SfM solution, shown to produce high detailed and robust reconstructions. An example of the reconstructed point clouds for grit size P40, can be seen in Figure 1(b).

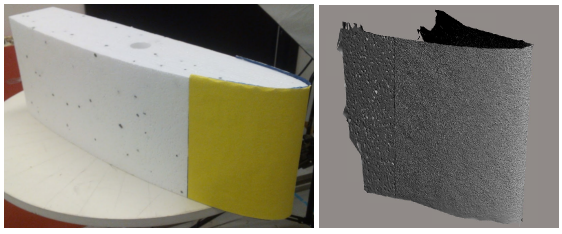

(a) (b)

Figure 1: Example of styrofoam blade replica with sandpaper of P40 installed on it 1(a), together with the reconstructed surface 1(b).

3.3 Sandpaper Feature Extraction

We extract a number of features from the sandpaper point clouds, as presented in the work by (Blomley et al., 2016). To calculate these features first the local neighbourhood around each point needs to be extracted, using a KDtree (Bentley, 1975), using the implementation from (Zhou et al., 2018). In their work (Blomley et al., 2016) and (Weinmann et al., 2015) test features extracted from different types of neighbourhood selection for each point. From the results of their work it can be seen that a combination of multiple neighbourhoods with different shapes and sizes gives the best results. We also choose this approach, but focus on neighbourhoods of the same shape, as the classes we are trying to detect, have uniform sandpaper roughness structures. We choose the neighbourhood scales, in a way that they can encompass the average particle sizes of the selected sandpaper grits. We choose spherical neighbourhoods with radii in the interval $[1 \dots 0.1]$ mm and a delta change of 0.1 mm. This creates 10 progressively smaller scales of neighbourhoods. If not enough points are present in the neighbourhood for calculating the features, it is zeroed out.

Three types of features are selected, as described in (Blomley et al., 2016) and (Weinmann et al., 2015), (Dittrich et al., 2017) - fundamental geometrical properties of the point clouds, local shape covariance features and local statistical shape distribution features. These are calculated for each neighbourhood scale and combined. As described by (Blomley et al., 2016), the fundamental geometrical properties are as follow:

- Local point density of the neighbourhood around a given point (Figure 2(a)),
- The farthest distance between points in the neighbourhood (Figure 2(b)),
- The maximum height of difference between points in the neighbourhood, where height is expressed in the direction of the average normal of the neighbourhood (Figure 2(c)),
- The standard deviation of the height differences between points in the neighbourhood, where again the height is expressed in the direction of the average normal (Figure 2(d)).

A visualization of these features for a neighbourhood size of 1*mm* on the P40 sandpaper are shown in Figure 2, where just a small area of the whole sandpaper leading edge is visualized.

The local shape features proposed by (Blomley et al., 2016) and (Weinmann et al., 2015) are based on the use of covariance features and require the calculation of the eigenvalues $\lambda_1, \lambda_2, \lambda_3$ of each neighbourhood scale. These features are as follows:

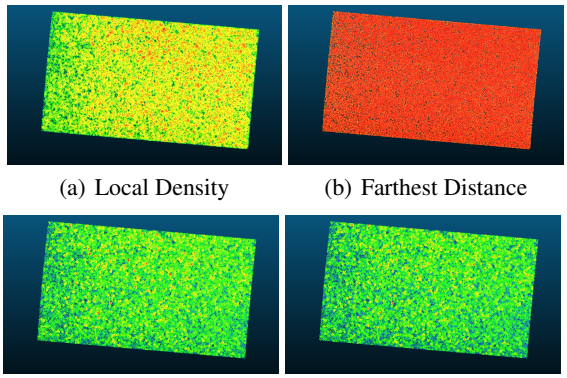

(a) Local Density (b) Farthest Distance

(c) Maximum Height (d) Height Std. Dev.

Figure 2: Example local fundamental geometrical properties, extracted from the P40 sandpaper grit size. Just a small part of the sandpaper leading edge is shown for easier visualization.

$$\text{Linearity: } L_\lambda = \frac{\lambda_1 - \lambda_2}{\lambda_1} \tag{1}$$

$$\text{Planarity: } P_\lambda = \frac{\lambda_2 - \lambda_3}{\lambda_1} \tag{2}$$

$$\text{Sphericity: } S_\lambda = \frac{\lambda_3}{\lambda_1} \tag{3}$$

$$\text{Omnivariance: } O_\lambda = \sqrt[3]{\prod_{i=1}^{3} \lambda_i} \tag{4}$$

$$\text{Anisotropy: } A_\lambda = \frac{\lambda_1 - \lambda_3}{\lambda_1} \tag{5}$$

$$\text{Eigenentropy: } E_\lambda = -\sum_{i=1}^{3} \lambda_i \ln \lambda_i \tag{6}$$

$$\text{Sum of Eigenvalues: } \Sigma_\lambda = \sum_{i=1}^{3} \lambda_i \tag{7}$$

$$\text{Local surface variation: } C_\lambda = \frac{\lambda_3}{\sum_{i=1}^{3} \lambda_i} \tag{8}$$

To calculate the eigenvalues, we first calculate the covariance matrix, of the points inside of the neighbourhood and extract the eigenvalues from it, which are then sorted in descending order. Example of how these features look on a P40 sandpaper, calculated from a neighbourhood size of $1mm$ is given in Figure 3.

The third type of features are the statistical shape distributions. These distributions are derived from the work by (Osada et al., 2002), for parameterization of the whole object's shape, but for use as local features, they can be used on neighbourhoods of points. These distributions are calculated as histograms of randomly sampled shape values. These shape values are based on five metrics:

- **D1** - distance from the neighbourhood centroid, to a random point from the same neighbourhood 4(a),
- **D2** - distance between two random points from the neighbourhood 4(b),
- **D3** - the square root of the area between three random points from the neighbourhood 4(c),
- **D4** - the cubic root of the volume of a tetrahedron made from four random points from the neighbourhood 4(d),
- **A3** - the angle between three random points from the neighbourhood 4(e).

We follow the suggestions by (Weinmann et al., 2015) and calculate the distributions as histograms with 10 bins and 255 random samplings from each neighbourhood scale. These results in 100 statistical distribution features per point. The visualization of the five used metrics, can be seen in Figure 4.

These features are extracted from each of the reconstructed sandpaper patches and used to train a Random Forest classifier. The same classifier is used in the work of (Weinmann et al., 2015) and (Nikolov and Madsen, 2020) and is proven to provide good results, when used with 3D surface features.

4 EXPERIMENTAL SCENARIOS AND RESULTS

Initially a simple classification scenario is test, using control reconstructed sandpaper patches. These patches are then classified by the trained Random Forest algorithms, to prove that the selected features can describe the surface of sandpaper patches of different grit size. After that a second testing scenario is proposed, using decommissioned wind turbine blades and classifying their surface depending on how close it resembles different sand paper grits.

The control sandpaper patches are from a different brand and represent again three different grit sizes - a rough large grit size P40, a medium grit size P80 and a fine small grit size P180. They are reconstructed using the same capturing protocol given in Subsection 3.2. The reconstructions are shown in Figure 5. These reconstructions are then used as testing data, to determine if the chosen features could describe unknown sandpaper surfaces, before transferring the knowledge to blade surfaces. The prediction results are given in Table 2. It can be seen that the highest percentage prediction for each of the testing sandpaper patches, showed in bold, corresponds to the real grit size of

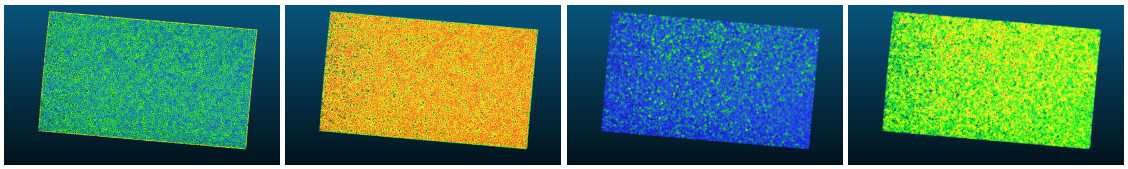

(a) Linearity (b) Planarity (c) Sphericity (d) Omnivariance

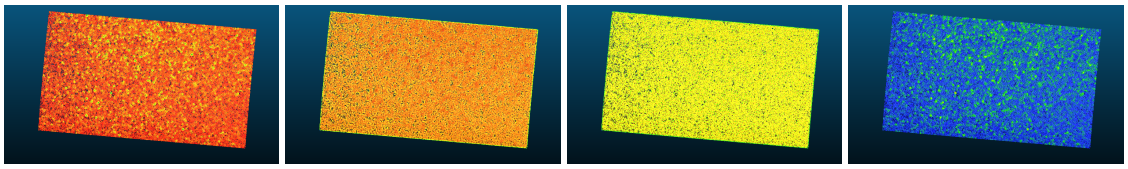

(e) Anisotropy (f) Eigentropy (g) Sum of Eigenvalues (h) Local Surface Variation

Figure 3: Example local covariance features, extracted from the P40 sandpaper grit size. Just a small part of the sandpaper leading edge is shown for easier visualization.

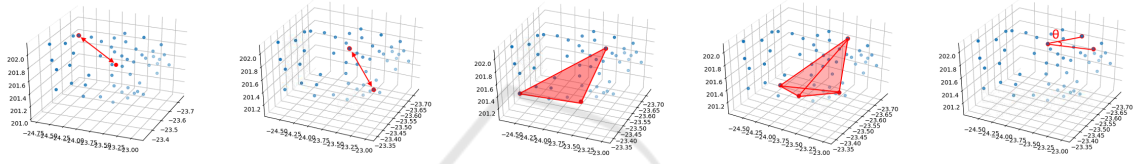

(a) D1 (b) D2 (c) D3 (d) D4 (e) A3

Figure 4: The five density metrics, used to calculate the statistical shape distributions, as proposed by (Osada et al., 2002).

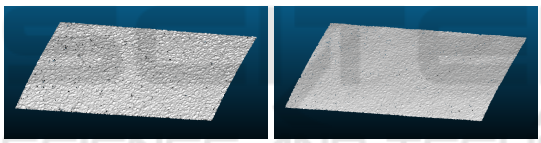

(a) P40 (b) P80

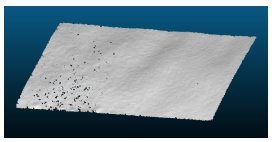

(c) P180

Figure 5: The three sandpaper patches, used as an initial test for how good are the used features for describing the sandpaper surface.

that patch. Some of the other grit sizes are also detected, as each of the patches contains smoother and rougher areas. For the P180, some problems come from the possible present reconstruction noise and low frequency surface roughness (Figure 5(c)), which can be classified as higher grit sizes.

For the second testing scenario three wind turbine blades, with varying surface roughness are selected. All the selected blades have been decommissioned and contain both smooth and very rough and damaged surface patches. One is a full blade, from which a number of patches are selected for reconstruction and the other two are smaller blade segments, which are used whole for the experiments. Four patches are selected from the full blade - two representing damaged and very rough areas and two representing relatively clean areas, with small amounts of surface roughness. The large blade, together with the two blade segments are shown in Figure 6.

Table 2: Results from the initial sandpaper data test, showing predictions for the three tested grit sizes P40, P80, P180 (horizontally). All three have been correctly predicted.

Grit Size	P40	P80	P180
P40	**0.761**	0.013	0.002
P60	0.193	0.127	0.101
P80	0.029	**0.696**	0.010
P100	0.007	0.055	0.059
P120	0.003	0.104	0.253
P180	0.007	0.005	**0.575**

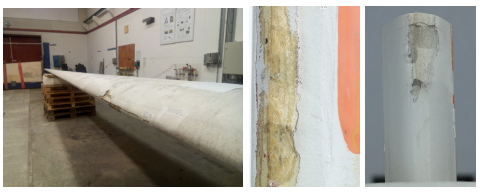

(a) (b) (c)

Figure 6: The three wind turbine blades used for the second experiment. Four patches with varying degree of roughness are selected from the first large blade (Figure 6(a)), while the other two segments (Figure 6(b) and 6(c)) are used whole.

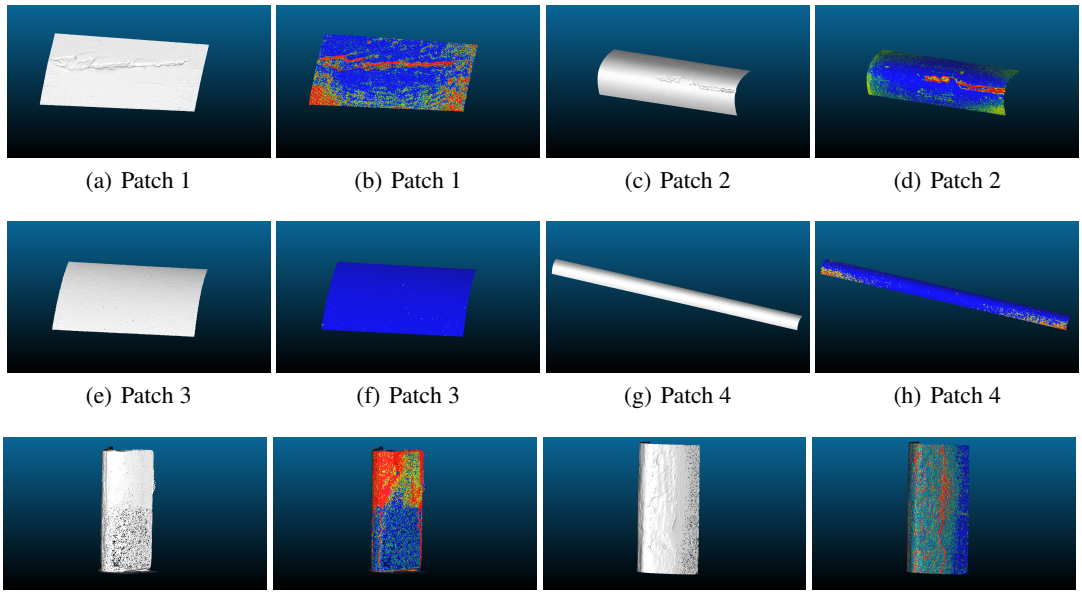

(a) Patch 1 (b) Patch 1 (c) Patch 2 (d) Patch 2

(e) Patch 3 (f) Patch 3 (g) Patch 4 (h) Patch 4

(i) Segment 1 (j) Segment 1 (k) Segment 2 (l) Segment 2

Figure 7: Results from segmentation of the wind turbine blades, visualized in pseudocolor, where P40 grit is shown as red and P180 is dark blue, while the other grit sizes are the colors between them. Just the point cloud is also given for each, for easier visualization of the roughness.

The four patches and two blade segments are reconstructed using Metashape, following the same capturing protocol presented in Subsection 3.2. The selected features, presented in 3.3, are extracted from the blade reconstructions and used as testing data for the Random Forest classifier. The result point clouds with pseudocolor information, on which sandpaper roughness best describes each point is given in Figure 7. The P40 grit size is shown as red color and the P180 as dark blue color, with all other grit sizes represented with the in-between colors.

Because there is no ground truth for calculating the accuracy of the surface classification, the roughness of each of the blade segments is first calculated as the distance to a best fitting plane. Each plane is fit to a spherical neighbourhood, which has been heuristically selected to best describe all parts of the point cloud. This is done through the use of the roughness calculation functionality of CloudCompare (Girardeau-Montaut, 2011). The distance between this roughness and our proposed method is then computed for each point. The nominal average diameter of the sandpaper grains given in Table 3.2 is used. We then calculate their root mean square error (RMSE) and standard deviation, which would give an overview of how good the sandpaper roughness is fit to the blade surface. These values are presented in Table 3. It can be seen that the damaged surface parts are mostly classified as a P40 grit, with the parts that have varying degrees of roughness classified as the smaller grit sizes. The P60 and P120 have the least amount of point classified as them. The smooth and clean surfaces, especially on the two patches (Figure 7(f) and 7(h)) and on the blade segments are represented with P180 grit size. From Table 3 it can be seen that on average the rougher patches exhibit a higher RMSE between the sandpaper representation and the real roughness. The blade segments on Figure 7(j) has a larger RMSE value, because the damages on it exhibit roughness values, which far exceed the values of the sandpaper grits. This testing scenario can be very dependent on the selected parameters and additional testing is required, with examples presented in the Future Work section 5.

Table 3: RMSE and standard deviation between the best fitting plane roughness calculation and our proposed solution.

	RMSE $[mm]$	Std. Dev. $[mm]$
Patch 1	0.179	0.113
Patch 2	0.125	0.069
Patch 3	0.070	0.009
Patch 4	0.101	0.060
Segment 1	0.162	0.110
Segment 2	0.288	0.122

5 CONCLUSION AND FUTURE WORK

In this paper we presented an idea for segmenting wind turbine blade surfaces depending on the sandpaper grit size that best represents their roughness. This solution aims to provide a standardized method classifying surface roughness of wind turbine blades that can be used for calculating their energy output and performance, as well as more easily modeling them for tests in wind tunnels.

We selected six different sandpaper patches with varying grit sizes and 3D reconstructed them using SfM. We then extracted a number of geometrical, covariance and statistical features from neighbourhoods with progressively smaller sizes. We used these features to train a Random Forest classifier.

To test the proposed solution we first evaluated the classier on a testing set of sandpaper patches. We verified that the extracted features could be used to identify each grit size of the training set. We then introduced surface data from three wind turbine blades. The data represented surfaces with varying degrees of surface roughness and damages. These surfaces were also 3D reconstructed and then used as a testing dataset. We demonstrated that we Random Forest classifier managed to sufficiently segment the surfaces and to represent their roughness as sandpaper grit sizes.

The current research lacks an in-depth verification of the robustness of the proposed methods. The next steps for the current research can be divided in two directions. The first direction requires the creation of ground truth 3D surface scans of the test blades and extracting the roughness from patches using a profilometer. These surfaces can then be used for more clear comparison to the proposed solution. The second direction would require the use of a wind tunnel, where the performance of a damaged blade and a blade with sandpaper of different grit sizes mounted on surfaces defined by the proposed algorithm can be compared.

REFERENCES

Agisoft (2010). Metashape. http://www.agisoft.com/. Accessed: 2019-09-20.

Al-Kaff, A., Moreno, F. M., San José, L. J., García, F., Martín, D., de la Escalera, A., Nieva, A., and Garcéa, J. L. M. (2017). Vbii-uav: Vision-based infrastructure inspection-uav. In *World Conference on Information Systems and Technologies*, pages 221–231. Springer.

Amenabar, I., Mendikute, A., López-Arraiza, A., Lizaranzu, M., and Aurrekoetxea, J. (2011). Comparison and analysis of non-destructive testing techniques suitable for delamination inspection in wind turbine blades. *Composites Part B: Engineering*, 42(5):1298–1305.

Bak, C., Gaunaa, M., Olsen, A. S., and Kruse, E. K. (2016). What is the critical height of leading edge roughness for aerodynamics. In *Journal of Physics: Conference Series*, volume 753, page 022023.

Bentley, J. L. (1975). Multidimensional binary search trees used for associative searching. *Communications of the ACM*, 18(9):509–517.

Blomley, R., Jutzi, B., and Weinmann, M. (2016). Classification of airborne laser scanning data using geometric multi-scale features and different neighbourhood types. *ISPRS Annals of Photogrammetry, Remote Sensing & Spatial Information Sciences*, 3(3).

Chan, C. H. L., Wang, Q., Holden, R., Huang, S., and Zhao, W. (2019). Optimal number of control points for fitting b-splines in wind turbine blade measurement. *International Journal of Precision Engineering and Manufacturing*, 20(9):1507–1517.

Chen, X. (2018). Fracture of wind turbine blades in operation—part i: A comprehensive forensic investigation. *Wind Energy*, 21(11):1046–1063.

Dastoorian, R., Elhabashy, A. E., Tian, W., Wells, L. J., and Camelio, J. A. (2018). Automated surface inspection using 3d point cloud data in manufacturing: A case study. In *International Manufacturing Science and Engineering Conference*, volume 51371, page V003T02A036. American Society of Mechanical Engineers.

Dittrich, A., Weinmann, M., and Hinz, S. (2017). Analytical and numerical investigations on the accuracy and robustness of geometric features extracted from 3d point cloud data. *ISPRS Journal of Photogrammetry and Remote Sensing*, 126:195–208.

Du, Y., Zhou, S., Jing, X., Peng, Y., Wu, H., and Kwok, N. (2020). Damage detection techniques for wind turbine blades: A review. *Mechanical Systems and Signal Processing*, 141:106445.

El-Mesery, H. S., Mao, H., and Abomohra, A. E.-F. (2019). Applications of non-destructive technologies for agricultural and food products quality inspection. *Sensors*, 19(4):846.

FEPA (1955). Fepa - federation of european producers of abrasives. https://www.fepa-abrasives.com/abrasive-products/grains. Accessed: 2019-03-06.

Genc, M. S., Kemal, K., and Açikel, H. H. (2019). Investigation of pre-stall flow control on wind turbine blade airfoil using roughness element. *Energy*, 176:320–334.

Girardeau-Montaut, D. (2011). Cloudcompare-open source project. *OpenSource Project*.

Hackel, T., Wegner, J. D., and Schindler, K. (2016). Fast semantic segmentation of 3d point clouds with strongly varying density. *ISPRS annals of the photogrammetry, remote sensing and spatial information sciences*, 3:177–184.

Han, W., Kim, J., and Kim, B. (2018). Effects of contamination and erosion at the leading edge of blade tip

airfoils on the annual energy production of wind turbines. *Renewable energy*, 115:817–823.

ISO25178 (2012). Iso25178(2012) geometrical product specifications (gps) — surface texture: Areal — part 2: Terms, definitions and surface texture parameters. https://www.iso.org/obp/ui/#iso:std:iso:25178:-2:ed-1:v1:en. Accessed: 2020-08-03.

ISO4287 (1997). Iso4287(1997) geometrical product specifications (gps) — surface texture: Profile method — terms, definitions and surface texture parameters. https://www.iso.org/standard/10132.html. Accessed: 2020-08-03.

ISO6344 (1998). Iso6344(1998) coated abrasives — grain size analysis parts 1-3. https://www.iso.org/standard/12643.html. Accessed: 2020-08-03.

Langel, C. M., Chow, R., Hurley, O. F., Van Dam, C. C. P., Maniaci, D. C., Ehrmann, R. S., and White, E. B. (2015). Analysis of the Impact of Leading Edge Surface Degradation on Wind Turbine Performance. In *33rd Wind Energy Symposium*, Reston, Virginia. American Institute of Aeronautics and Astronautics.

Langel, C. M., Chow, R., Van Dam, C., and Maniaci, D. C. (2017). Rans based methodology for predicting the influence of leading edge erosion on airfoil performance. Technical report, Sandia National Lab.(SNL-NM), Albuquerque, NM (United States).

Lowe, D. G. (2004). Distinctive image features from scale-invariant keypoints. *International journal of computer vision*, 60(2):91–110.

Martin, R. W., Sabato, A., Schoenberg, A., Giles, R. H., and Niezrecki, C. (2018). Comparison of nondestructive testing techniques for the inspection of wind turbine blades' spar caps. *Wind Energy*, 21(11):980–996.

Marzuki, O. F., Rafie, A. S. M., Romli, F. I., and Ahmad, K. A. (2018). Magnus wind turbine: the effect of sandpaper surface roughness on cylinder blades. *Acta Mechanica*, 229(1):71–85.

Moreno, S., Peña, M., Toledo, A., Treviño, R., and Ponce, H. (2018). A new vision-based method using deep learning for damage inspection in wind turbine blades. In *2018 15th International Conference on Electrical Engineering, Computing Science and Automatic Control (CCE)*, pages 1–5. IEEE.

Nielsen, M., Nikolov, I., Kruse, E., Garnæs, J., and Madsen, C. (2020). High-resolution structure-from-motion for quantitative measurement of leading-edge roughness. *Energies*, 13(15).

Nikolov, I. and Madsen, C. (2016). Benchmarking close-range structure from motion 3d reconstruction software under varying capturing conditions. In *Euro-Mediterranean Conference*, pages 15–26. Springer.

Nikolov, I. and Madsen, C. (2020). Rough or noisy? metrics for noise estimation in sfm reconstructions. *Sensors*, 20(19):5725.

Osada, R., Funkhouser, T., Chazelle, B., and Dobkin, D. (2002). Shape distributions. *ACM Transactions on Graphics (TOG)*, 21(4):807–832.

Ozyesil, O., Voroninski, V., Basri, R., and Singer, A. (2017). A survey of structure from motion. *arXiv preprint arXiv:1701.08493*.

Peng, L. and Liu, J. (2018). Detection and analysis of large-scale wt blade surface cracks based on uav-taken images. *IET Image Processing*, 12(11):2059–2064.

Rublee, E., Rabaud, V., Konolige, K., and Bradski, G. (2011). Orb: An efficient alternative to sift or surf. In *2011 International conference on computer vision*, pages 2564–2571. Ieee.

Schramm, M., Rahimi, H., Stoevesandt, B., and Tangager, K. (2017). The Influence of Eroded Blades on Wind Turbine Performance Using Numerical Simulations. *Energies*, 10(9):1420.

Shihavuddin, A., Chen, X., Fedorov, V., Nymark Christensen, A., Andre Brogaard Riis, N., Branner, K., Bjorholm Dahl, A., and Reinhold Paulsen, R. (2019). Wind turbine surface damage detection by deep learning aided drone inspection analysis. *Energies*, 12(4):676.

Triggs, B., McLauchlan, P. F., Hartley, R. I., and Fitzgibbon, A. W. (1999). Bundle adjustment—a modern synthesis. In *International workshop on vision algorithms*, pages 298–372. Springer.

Wang, L. and Zhang, Z. (2017). Automatic Detection of Wind Turbine Blade Surface Cracks Based on UAV-Taken Images. *IEEE Transactions on Industrial Electronics*, 64(9):7293–7303.

Weinmann, M., Jutzi, B., Hinz, S., and Mallet, C. (2015). Semantic point cloud interpretation based on optimal neighborhoods, relevant features and efficient classifiers. *ISPRS Journal of Photogrammetry and Remote Sensing*, 105:286–304.

Xu, D., Wen, C., and Liu, J. (2019). Wind turbine blade surface inspection based on deep learning and uav-taken images. *Journal of Renewable and Sustainable Energy*, 11(5):053305.

Zhang, D., Burnham, K., Mcdonald, L., Macleod, C., Dobie, G., Summan, R., and Pierce, G. (2017a). Remote inspection of wind turbine blades using uav with photogrammetry payload. In *56th Annual British Conference of Non-Destructive Testing-NDT 2017*.

Zhang, D., Watson, R., Dobie, G., MacLeod, C., Khan, A., and Pierce, G. (2020). Quantifying impacts on remote photogrammetric inspection using unmanned aerial vehicles. *Engineering Structures*, page 109940.

Zhang, Y., Yuan, X., Fang, Y., and Chen, S. (2017b). Uav low altitude photogrammetry for power line inspection. *ISPRS International Journal of Geo-Information*, 6(1):14.

Zhou, Q.-Y., Park, J., and Koltun, V. (2018). Open3D: A modern library for 3D data processing. *arXiv:1801.09847*.